Evidence for the First Misfit Layer Oxide $Tl_{0.41}(Sr_{0.9}O)_{1.12}CoO_2$

Philippe Boullay, Bernadette Domengès, Maryvonne Hervieu,* Daniel Groult, and Bernard Raveau

Laboratoire CRISMAT-ISMRA, URA 1318 associé au CNRS, ISMRA et Université de Caen, Bd Maréchal Juin, 14050 Caen Cedex, France

Received February 1, 1996. Revised Manuscript Received May 3, 1996[⊗]

A misfit layer oxide $Tl_{0.41}(Sr_{0.9}O)_{1.12}CoO_2$ has been synthesized, and its structural model established by ED and HREM. The cell parameters of the two subsystems have been refined from XRPD data. The subsystem S_1 (a = 4.9498(5) Å, b_1 = 5.0222(6) Å, c = 11.656(1) Å, β = 97.755(7)°) characterizes the strontium-deficient rock-salt layers $[(Sr_{0.9}\square_{0.1})O]_\infty$, whereas the subsystem S_2 (a = 4.9498(5) Å, b_2 = 2.807(2) Å, c = 11.656(1) Å, β = 97.755(7)°) corresponds to the octahedral $[CoO_2]_\infty$ layers that exhibit the CdI_2 structure. The thallium atoms are located between the two kinds of layers, with a distorded tetrahedral coordination, ensuring the cohesion of the structure.

Introduction

The recent studies of the superconducting layered cuprates have shown the great ability of $[MO]_\infty$ rock-salt layers with M = Sr, Ca, Bi, Tl, Pb, Ln to be adapted to another type of structural units leading to numerous series of intergrowths between the rock-salt and perovskite structures (see for a review ref 1). As an example, in the so-called 1201 structure one $[TlO]_\infty$ layer is sandwiched between two $[SrO]_\infty$ layers to form a double rock-salt layer. This unit is intergrown with a single perovskite layer where Cu cations[2] and Co[3] can occupy the octahedral sites. Similarly to the cuprates, many transition-metal sulfides exhibit a layer structure built up from $[MS]_\infty$ rock-salt type layers, but in contrast to the oxides they are not intergrown with perovskite layers. When the rock salt layers $[MS]_\infty$ are stacked with $[TS_2]_\infty$ layers with the CdI_2 structure, they form a large series of misfit compounds $[MS]_{1+x}[TS_2]$ with M = Ln, Pb, Bi, Sn and T = Ti, V, Cr (see for a review ref 4).

The inability of cuprates to form such misfit structures can be explained by the Jahn−Teller properties of copper, which may prevent close-packed octahedral $[CuO_2]_\infty$ layers with a CdI_2 type structure to be formed. In this respect, cobalt appears as a promising candidate for the generation of oxides with such misfit structures, due to the fact that the oxides Na_xCoO_2[5] or $LiCoO_2$[6] exhibit $[CoO_2]_\infty$ layers with the CdI_2 type structure. To generate such frameworks, cobalt should be associated with cations such as strontium and thallium, so that $[SrO]_\infty$ and $[TlO]_\infty$ layers can be formed.

For this reason, a systematic investigation of the Tl−Sr−Co−O system was performed. We report herein on the synthesis and structural study of the first oxide with a misfit layer structure, $Tl_{0.41}(Sr_{0.9}O)_{1.12}CoO_2$.

Experimental Section

Synthesis. The new compound was synthesized in two steps: first a mixture of Co_3O_4 and $SrCO_3$ was ground in an agate mortar and heated in air at 950 °C for 24 h for decarbonation. Tl_2O_3 was then added in order to realize the nominal composition "$Tl_{0.6}SrCoO_y$"; after intimate grinding, the powder was packed in an alumina finger and sealed in an evacuated silica tube. The samples were heated at 880 °C for 20 h and slowly cooled to room temperature.

Electron Microscopy Study. Powders were gently ground in an agate mortar in *n*-butanol and deposited on a holey carbon coated copper grid or on an uncoated grid previously dipped in an adhesive solution. Electron diffraction (ED) was performed on a JEM200CX electron microscope equipped with a tilting rotating goniometer (±60°) and high-resolution study was performed on a TOPCON 002B electron microscope equipped with a ±10° double-tilt goniometer and an objective lens with spherical aberration constant of 0.4 mm. Both microscopes are equipped with KEVEX EDS analyzers. High-resolution images (HREM) were simulated using the multislice method of the EMS package.

Powder X-ray Diffraction Study. The X-ray powder diffraction patterns (XRPD) were registered on a Seifert diffractometer using the Cu $K\alpha_1$ radiation from 5° to 80° (2θ) in 0.02° steps. The data were studied in a profile matching mode with the program Fullprof (version 3.1).

Results and Discussion

For the nominal composition $Tl_{0.6}SrCoO_y$, the XRPD pattern evidences the formation of a new phase. The EDS analyses performed on numerous crystallites show that they all exhibit the same cationic composition, "$Tl_{0.43\pm0.03}Sr_{1\pm0.06}Co_{1\pm0.06}O_y$", involving a significant thallium loss with respect to the nominal one.

The electron microscopy investigation reveals the mica like morphology of the crystals, so that most of the crystallites exhibit a similar orientation. The cor-

[⊗] Abstract published in *Advance ACS Abstracts,* June 15, 1996.

(1) Raveau, B.; Michel, C.; Hervieu, M.; Groult, D. *Crystal Chemistry of High-Tc Superconducting Copper Oxides*; Springer Series in Materials Science 15; Springer-Verlag: Berlin, 1991.

(2) Kim, J. S.; Swinnea, J. S.; Steinfink, H. *J. Less Common Met.* **1989**, *156*, 347.

(3) Contanceau, M.; Dorder, P.; Doumerc, J. P.; Grenier, J. L.; Maestro, P.; Pouchard, M.; Sedmidubsky, D.; Seguelong, T. *Solid State Commun.* **1995**, *96*, 569.

(4) Wiegers, G. A.; Meerschaut, A. *J. Alloys Compounds* **1992**, *178*, 351.

(5) Fouassier, C.; Mateska, G.; Reau, J. M.; Hagenmuller, P. *J. Solid State Chem.* **1973**, *6*, 532.

(6) Orman, H. J.; Wiseman, P. J. *Acta Crystallogr.* **1984**, *C40*, 12.

(7) Rodriguez-Carjaval, J. Proc. Satellite Meeting on Powder Diffraction of the XVth Congress of Int. Union of Crystallography, Toulouse, France, July 1990.

S0897-4756(96)00144-5 CCC: $12.00

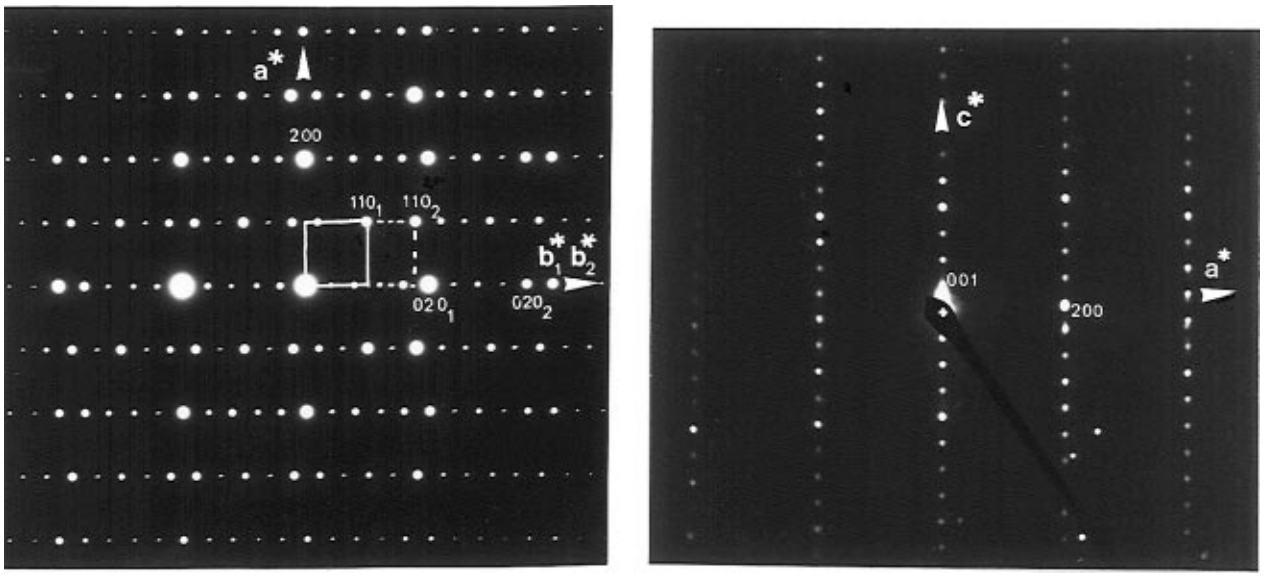

Figure 1. $Tl_{0.41}[(Sr_{0.9}\square_{0.1})O]_{1.12}CoO_2$ compound: (a, left) (001)* ED pattern. The two subsystems are indexed 1 and 2. The two subcells are outlined (white line for S_1 and dotted lines for S_2). (b, right) (010)* ED pattern, which is the common plane to the two subsystems. The conditions limiting the reflection are hkl: $h + k = 2n$.

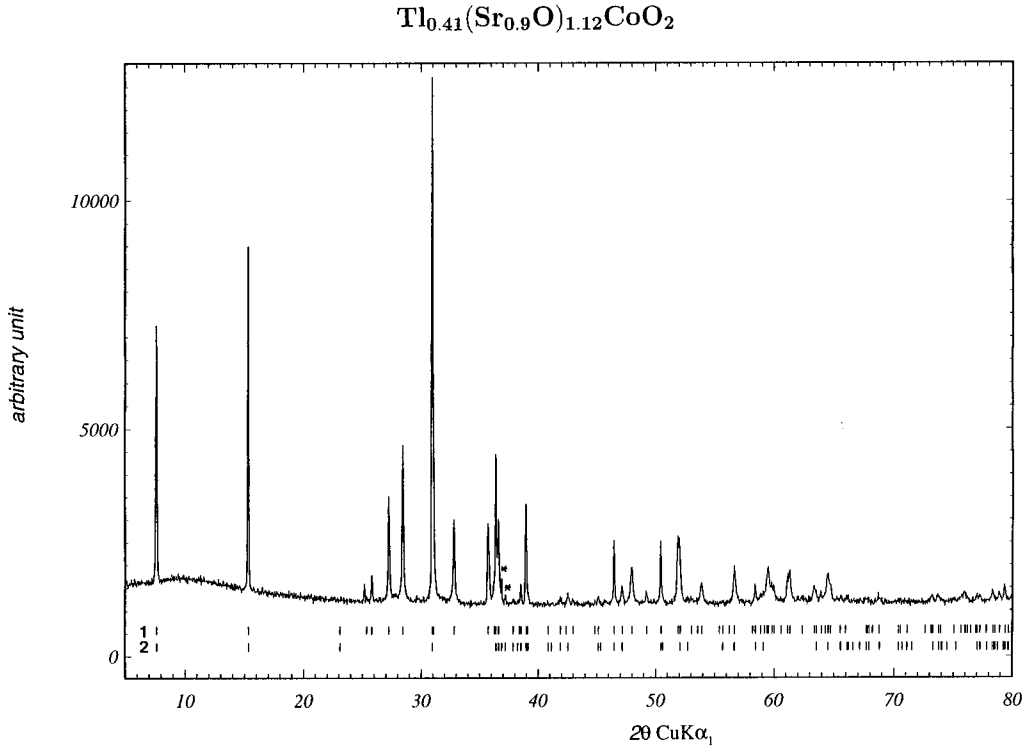

Figure 2. $Tl_{0.41}[(Sr_{0.9}\square_{0.1})O]_{1.12}CoO_2$: X-ray powder diffraction pattern. The first subsystem reflections (S1) and the second subsystem reflections (S2) are marked out 1 and 2, respectively. Only two reflections of the second subsystem are not common with those of the first one; they are indicated by asterisks.

responding ED patterns show that two sets of main reflections systematically coexist, as shown for the (001)* plane in Figure 1a, where the two corresponding systems are indexed 1 and 2. Only the main reflections of the two subsystems are indexed. Both are centered and exhibit a common a^* axis; $\vec{b}_1^*$ and $\vec{b}_2^*$ are normal to $\vec{a}^*$. The reconstruction of the reciprocal space was performed rotating about $\vec{b}^*$. The observed conditions of reflection are hkl: $h + k = 2n$.

Both subsystems have a monoclinic unit cell with a C-type lattice. The common plane is (a^*c^*) (Figure 1b). In this (010)* ED pattern only one set of reflections is observed corresponding to the common $h0l$ reflections. These two subsystems can be defined with their own 3D translation vectors:

$$S_1 = \{\vec{a},\vec{b}_1,\vec{c}\} \quad \text{with } a \simeq 4.95 \text{ Å}, \; b_1 \simeq 5.02 \text{ Å}, \; c \simeq 11.66 \text{ Å}, \; \beta \simeq 97.76°$$

$$S_2 = \{\vec{a},\vec{b}_2,\vec{c}\} \quad \text{with } a \simeq 4.95 \text{ Å}, \; b_2 \simeq 2.81 \text{ Å}, \; c \simeq 11.66 \text{ Å}, \; \beta \simeq 97.76°$$

In fact the latter subsystem, S_2, can be described using a trigonal symmetry, but for convenience we retain the monoclinic cell to make easier the geometrical

Table 1. Lattice Parameters

$Tl_{0.41}(Sr_{0.9}O)_{1.12}CoO_2$		$(PbS)_{1.18}TiS_2$ (from ref 10[a])	
subsystem 1 (S_1)	subsystem 2 (S_2)	subsystem 1 (S_1)	subsystem 2 (S_2)
SG: $C2/m$	SG: $C2/m$	SG: $C2/m$	Sg:$C2/m$
$a = 4.9498(5)$ Å	$a = 4.9498(5)$ Å	$a = 5.881(1)$ Å	$a = 5.880(2)$ Å
$b_1 = 5.0222(6)$ Å	$b_2 = 2.807(2)$ Å	$b_1 = 5.800(2)$ Å	$b_2 = 3.409(1)$ Å
$c = 11.656(1)$ Å	$c = 11.656(1)$ Å	$c = 11.759(2)$ Å	$c = 11.760(2)$ Å
$\beta = 97.755(7)°$	$\beta = 97.755(7)°$	$\beta = 95.27(2)°$	$\beta = 95.29(2)°$
$r = b_1/b_2 \simeq 1.789$ close to $^9/_5$		$r = b_1/b_2 \simeq 1.7$ close to $^7/_4$	
centering translation $(^1/_2,^1/_2,0,^1/_2)$		centering translation $(^1/_2,^1/_2,0,^1/_2)$	
IR_4 Laue class: $C2/m(0,r,0)$		SSG: $P_{s1}^{C2/m}(0,r,0)$ *or* $P_{1\bar{1}}^{C2/m}(0,r,0)$	

[a] In the original paper $\vec{a}$ is the unique axis.

relationships between the two subsystems. The ratio between b_1 and b_2 of the monoclinic cells is incommensurate and expressed by $r = b_1/b_2 \simeq 1.789$ and the closest corresponding simple fraction is $^9/_5$. The strain induced by the mismatch of the layers along $\vec{b}$ can then be expressed by $(^9/_5 - b_1/b_2)/^9/_5$ and corresponds to 0.6%.

The XRPD pattern of this phase (Figure 2) has been indexed on the basis of these observations. The lattice parameters of both subsystems can be refined, using the ED results as starting values (Table 1). In the bottom part of the Figure 2 the reflections corresponding to each subsystem are marked. The *h*0*l* reflections common to both subsystems are the most intenses reflections. Obviously most of the reflections can be indexed with a sole monoclinic cell ($a \simeq 4.95$ Å, $b \simeq 5.02$ Å, $c \simeq 11.66$ Å, $\beta \simeq 97.76°$, space group $C2/m$) corresponding to the first subsystem S_1. For the second subsystem the *hkl* reflections with *k* not equal to zero are fewer because the value of the b_2 parameter is smaller. The two reflections which are unique to the second subsystem and cannot be indexed by the first subsystem are marked by asterisks in the figure.

These results show that this new phase is a composite structure, i.e., a structure where the *basic structure* consists of two or more subsystems having their own, but mutually incommensurate, 3D translation symmetry. The interactions between subsystems induce atomic displacive modulations in each subsystem and the *complete structure* consists of a set of modulated subsystems mutually incommensurate.[8]

In fact the parameter relationships and the highly lamellar character of the structure suggest that this compound belongs to a particular class of composite crystals called the "misfit layer structures" (see for a review ref 9). The latter result from the stacking of layered subsystems alternating in a direction normal or nearly normal to the layers which have periods incommensurate with each other. So in the plane of layers, here the (*ab*) plane, at least one of the two lattice parameters of one layer is incommensurate with a lattice parameter of the other layers (along the *b* axis in the present case).

In the present oxide, the reciprocal vectors of the first and second subsystems belong to the minimal set $M = \{\vec{a}^*,\vec{b}_1^*,\vec{c}^*,\vec{b}_2^*\}$ of reciprocal vectors required for indexing the complete ED patterns. Every vector $\vec{s}$ is expressed by $\vec{s} = h\vec{a}^* + k\vec{b}_1^* + l\vec{c}^* + m\vec{b}_2^*$. According to this notation, the first subsystem gives rise to *hkl*0 reflections and the second to *h*0*lm* reflections. From the reconstruction of the reciprocal space, the conditions

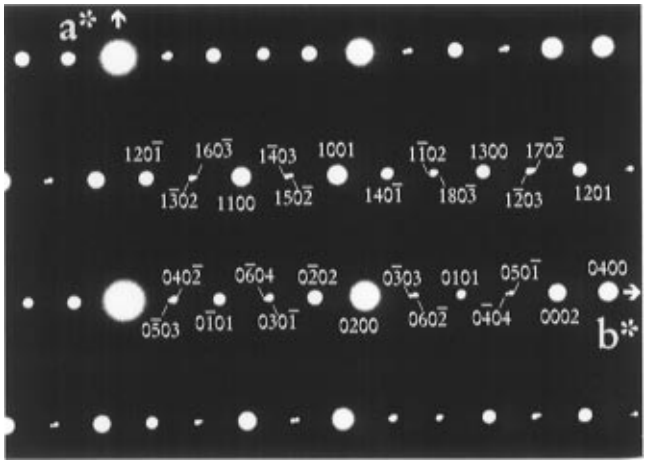

Figure 3. Indexation of the (0010)* plane in a quadridimensional formalism. The first subsystem gives rise to *hk*00 reflections while the second to *h*00*m* reflections. The *hk*0*m* reflections ($k \neq 0$ and $m \neq 0$) correspond to satellite reflections which are common to the two subsystems.

limiting the reflections are *hklm*: $h + k + m = 2n$. These conditions imply the centering translation ($^1/_2$, $^1/_2$, 0, $^1/_2$). As an example the indexation of the (*a***b**) plane is given using a 4-dimensional formalism (Figure 3). The first subsystem gives rise to *hk*00 reflections, while the second gives rise to *h*00*m* reflections. The *hk*0*m* reflections (with $h \neq 0$ and $k \neq 0$) correspond to satellite reflections which are common to the two subsystems.

The comparison of the cell parameters of the two S_1 and S_2 subsystems with those of the sulfides $[MS]_{1+x}[TS_2]$ (see Table 1 for M = Pb and T = Ti) supports strongly the hypothesis of a misfit structure built up from $[CoO_2]_\infty$ layers with the CdI_2 type structure, and $[SrO]_\infty$ layers with the rock-salt structure.

In the first subsystem S_1 the *a* and b_1 parameters of 4.95 and 5.02 Å, respectively are close to those of SrO ($a \simeq 5.1$ Å), in agreement with those observed for $(PbS)_{1.18}(TiS_2)$,[10] whose values of 5.88 and 5.8 Å, respectively, are close to those of PbS ($a \simeq 5.9$ Å). Thus the (ab_1) plane of S_1 is compatible with a {001} rock-salt $[SrO]_\infty$ layer (Figure 4a).

For the second subsystem S_2, the relationships between *a* and b_2, $b_2 \simeq a/\sqrt{3} \simeq 2.8$ Å, shows a pseudo-

(8) Janner, A.; Janssen, T. *Acta Crystallogr.* **1980**, *A36*, 408.
(9) Makovicky, E.; Hyde, B. G. *Struct. Bonding* **1981**, *46*, 11.
(10) Van Smaalen, S.; Meetsma, A.; Wiegers, G. A.; De Boer, J. L. *Acta Crystallogr.* **1991**, *B47*, 314.
(11) Rouxel, J.; Maelo, Y.; Lafond, A.; Disalvo, F. J.; Meerschaut, A.; Roesky, R. *Inorg. Chem.* **1994**, *33*, 3358.
(12) Michel, C.; Suard, E.; Caignaert, V.; Martin, C.; Maignan, A.; Hervieu, M.; Raveau, B. *Physica C* **1991**, *178*, 29.
(13) Onada, M.; Saeki, M.; Yamamoto, A.; Kato, K. *Acta Crystallogr.* **1993**, *B49*, 929.
(14) Ganal, P.; Moreau, P.; Ouvrard, G.; Sidorov, M.; McKelvy, M.; Glaunsinger, W. *Chem. Mater.* **1995**, *7*, 1132.

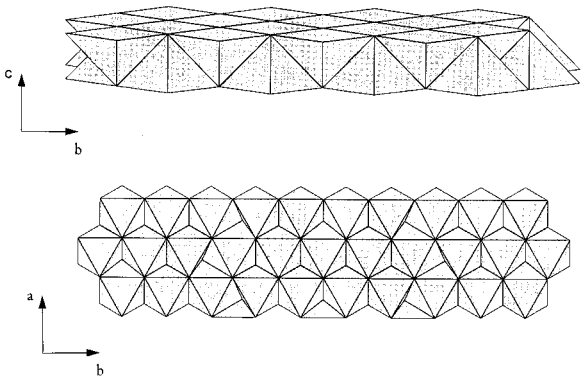

Figure 4. (a) Idealized drawing of the single rock-salt layer showing the strontium environment. (b) Idealized projection along [001] of one $[CoO_2]_\infty$ layer built up from edge-sharing octahedra $[CoO_6]$. The projected tetrahedral sites suitable for thallium atoms are represented as bright triangles.

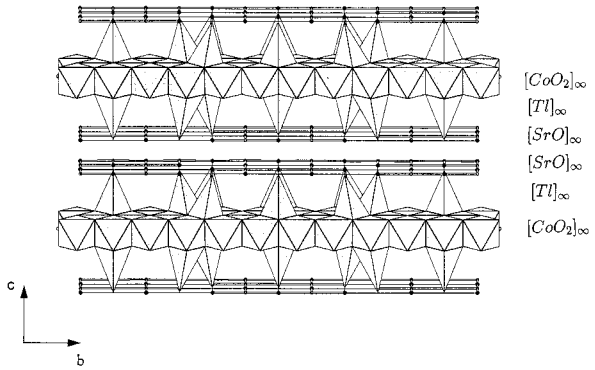

Figure 5. Idealized drawing of the $Tl_{0.66}[SrO]_{1.12}CoO_2$ structure viewed along $\vec{a}$.

hexagonal symmetry, which can be compared to the trigonal lattice observed for Na_xCoO_2 ($0.9 \leq x < 1$) or $LiCoO_2$ that exhibit an a parameter of 2.8−2.9 Å. Again, the similarity with $(PbS)_{1.18}(TiS_2)$, for which $b_2 \simeq a/\sqrt{3} \simeq 3.4$ Å corresponds to a pseudohexagonal lattice is also striking. Thus the (ab_2) plane of S_2 is compatible with a {001} $[CoO_2]_\infty$ layer built up from edge-sharing octahedra, i.e., with the CdI_2 type structure (Figure 4b). Finally the c parameter and the β angle, very similar to those observed in this sulfide, emphasize the great similarity with the misfit layer structures.

At this point, a chemical formulation can be proposed, based on the cationic composition deduced from the EDS analysis and taking into consideration the fact that in the misfit layer sulfides $[MS]_{1+x}[TS_2]$ the term $1 + x$ reflects the nonstoichiometry and is attached to the ratio of the two mutually incommensurate parameters, with $1 + x = 2b_{TS_2}/b_{MS}$ (considering the mesh fits along b). Considering the $1 + x = 2b_{CoO_2}/b_{SrO} \simeq 1.12$ deduced from the b_1 and b_2 parameters one obtains the theoretical formula $[SrO]_{1.12}[CoO_2]$ which differs significantly from the cationic composition "$Tl_{0.43}SrCo$" deduced from EDS and raises the issue of thallium location. On the basis of the fact that there exist misfit layer sulfides with cationic deficient rock-salt layers such as $[(Gd_{0.91}\square_{0.09})S]_{1.27}[CrS_2]$,[11] a similar behavior can be proposed for this oxide, leading finally to the formula $Tl_{0.41}[(Sr_{0.9}\square_{0.1})O]_{1.12}CoO_2$, which is in agreement with the cationic analysis in the limits of the error and implies with 0.41 Tl that thallium and cobalt are both trivalent.

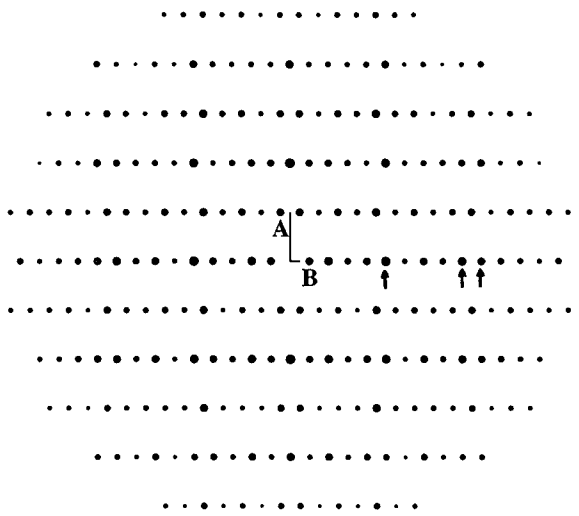

Figure 6. Calculated (001)* ED pattern for the positional parameters given in Table 2, and a crystal thickness of 4.7 nm.

The location of thallium is then easily understood by considering the view of the structure along [100] (Figure 5). Tetrahedral sites, located between the $[SrO]_\infty$ and $[CoO_2]_\infty$ layers are indeed available. Each tetrahedron has one face formed by three oxygen atoms of one $[CoO_2]_\infty$ layer, the fourth apex being provided by the adjacent $[SrO]_\infty$ layer. All potential tetrahedral sites existing on the surface of the $[CoO_2]_\infty$ layer can only be

Table 2. Atomic Positional Parameters for $Tl_{0.41}(Sr_{0.9}O)_{1.12}CoO_2$[a]

element	*x*	*y*	*z*	site	occupancy	element	*x*	*y*	*z*	site	occupancy
Sr1	0.025	0	0.89	2a	0.9	O1	0.02	0	0.11	2a	1
Sr2	0.025	0.2	0.89	4b	0.9	O2	0.02	0.2	0.11	4b	1
Sr3	0.025	0.4	0.89	4b	0.9	O3	0.02	0.4	0.11	4b	1
Sr4	0.025	0.5	0.11	2a	0.9	O4	0.02	0.5	0.89	2a	1
Sr5	0.025	0.7	0.11	4b	0.9	O5	0.02	0.7	0.89	4b	1
Sr6	0.025	0.9	0.11	4b	0.9	O6	0.02	0.9	0.89	4b	1
Co1	0	0	0.5	2a	1	O7	0.3	0	0.4	2a	1
Co2	0	0.111	0.5	4b	1	O8	0.3	0.111	0.4	4b	1
Co3	0	0.222	0.5	4b	1	O9	0.3	0.222	0.4	4b	1
Co4	0	0.333	0.5	4b	1	O10	0.3	0.333	0.4	4b	1
Co5	0	0.444	0.5	4b	1	O11	0.3	0.444	0.4	4b	1
Tl1	0.4	0	0.71	2a	0.615	O12	0.2	0.0555	0.6	4b	1
T12	0.4	0.222	0.71	4b	0.615	O13	0.2	0.1665	0.6	4b	1
T13	0.45	0.5	0.28	2a	0.615	O14	0.2	0.2775	0.6	4b	1
T14	0.45	0.7225	0.28	4b	0.615	O15	0.2	0.3885	0.6	4b	1
						O16	0.2	0.5	0.6	2a	1

[a] Model in an ideal commensurate supercell. SG: *Cm*, $a = 4.95$ Å, $b = 25.19$ Å, $c = 11.66$ Å, $\beta = 97.76°$.

$(SrO)_{1.12}CoO_2$

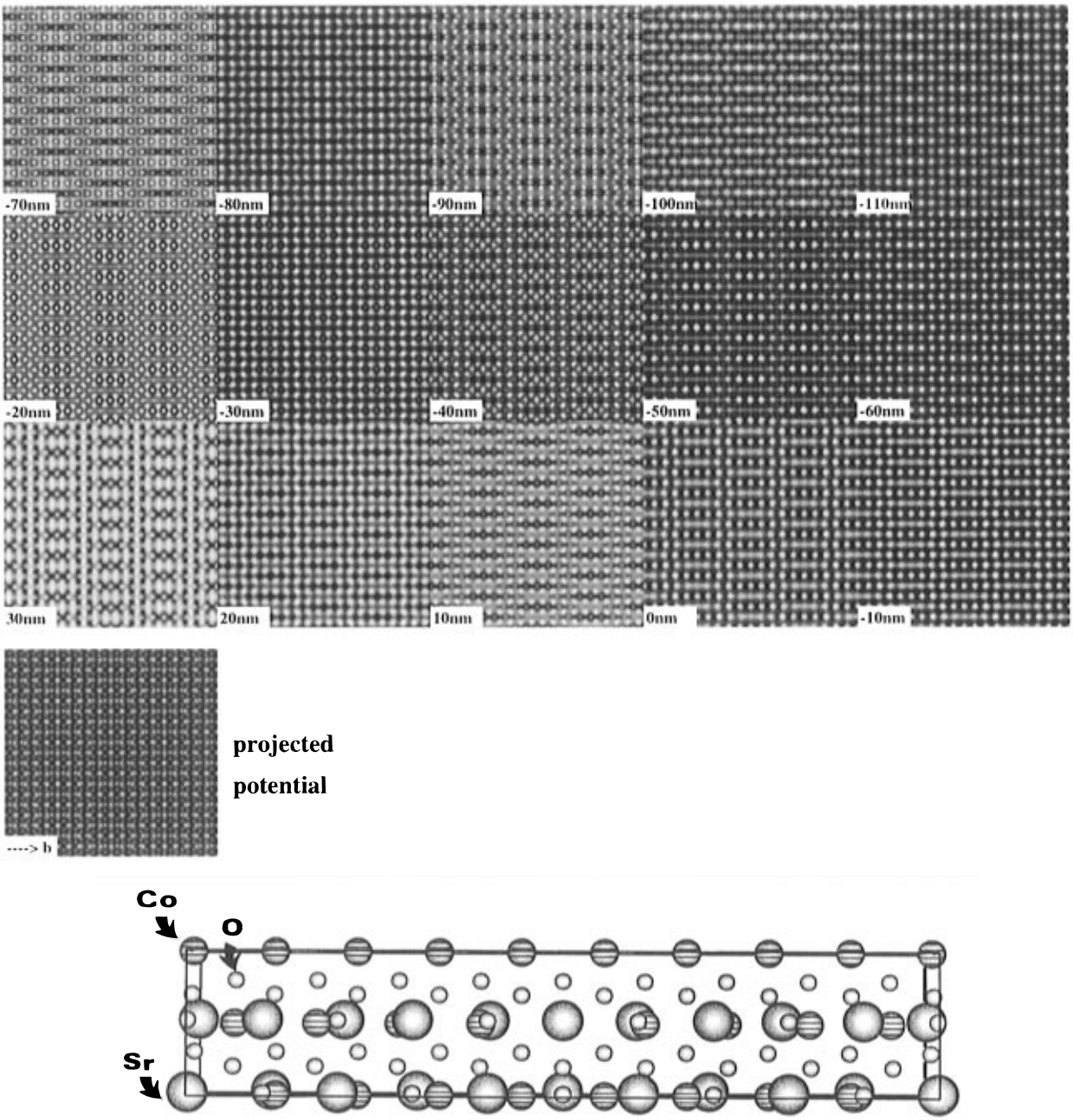

Figure 7. $[SrO]_{1.12}[CoO_2]$: (a, top left) calculated through focus series for focus ranging from 30 to −110 nm; (b, bottom left) corresponding projected structure. $Tl_{0.41}[(Sr_{0.9}\square_{0.1})O]_{1.12}CoO_2$: (c, top right) calculated through focus series for focus ranging from 30 to −110 nm; (d, bottom right) corresponding projected structure; simulation parameters: accelerating voltage $V = 200$ kV, crystal thickness $t = 4.7$ nm, $C_s = 0.4$ mm, objective aperture radius $R = 20$ nm^{-1}, spread of focus $\Delta = 10$ nm, beam half convergence $\alpha = 0.85$ mrad.

occupied when an oxygen of the $[SrO]_\infty$ layer is close enough to form the fourth bond of the tetrahedron. The possible TlO_4 tetrahedra, represented by bright triangles in Figure 4b, form rows parallel to $\vec{a}$; one single row of single sites alternates with one double row of staggered sites. The thallium positions are shifted by $(a + b)/2$, in agreement with the C-type lattice. The occurrence of such sites along the $\vec{b}$ direction depends on the incommensurate ratio between b_1 and b_2, so that a maximum occupancy corresponds to $x = 0.66$ per formula $Tl_x[(Sr_{0.9}\square_{0.1})O]_{1.12}CoO_2$. This occupation of tetrahedral sites by Tl(III) is in agreement with the great ability of this species to accommodate various distorted coordinations, and especially tetrahedral coordinations, as observed for instance in the cuprate $TlBa_2Ca_{1-x}Nd_xCuO_{7-\delta}$.[12] Moreover, the presence of thallium in those sites ensures the cohesion between the $[CoO_2]_\infty$ and the $[(Sr_{0.9}\square_{0.1})O]_\infty$ layers, explaining the stability of the structure. Nevertheless, the presence of Tl(III) in the $[(Sr_{0.9}\square_{0.1})O]_\infty$ layers cannot be ruled out, although less likely due to its smaller size compared to strontium.

The determination of such a structure from powder data using X-ray diffraction is still unusual[13,14] and

$Tl_{0.41}(Sr_{0.9}O)_{1.12}CoO_2$

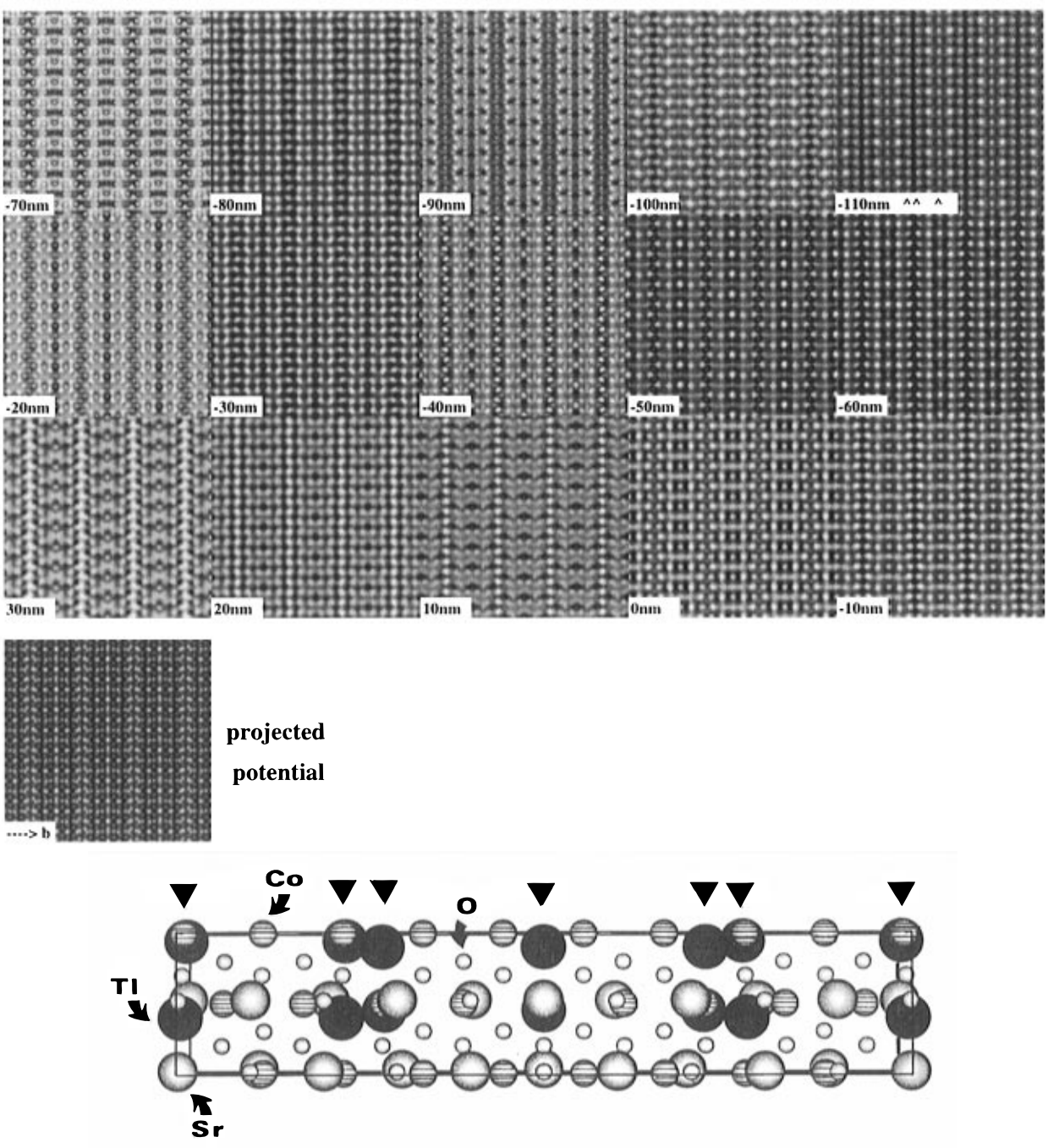

Figure 7. (continued).

requires two clearly distinct subsystems. In the present case, only two reflections of the second subsystem are not superposed to the first subsystem so that they do not provide enough information for such a determination.

To check the validity of our model ED patterns and HREM images were simulated. The positional parameters were deduced from an ideal model corresponding to $r = {}^9/_5$. The supercell parameters correspond to $a = a_1 = a_2$, $b \simeq 5b_1$, $\simeq 9b_2 \simeq 25.2$ Å, $c = c_1 = c_2$, and $\beta = 97.76°$. The atoms' coordinates are given in Table 2 for the *Cm* space group. The ED patterns were simulated for different crystal thicknesses, ranging between 4.7 and 20 nm. An example of (a^*b^*) plane is given in Figure 6 for a crystal thickness of 4.7 nm. It perfectly fits with the experimental ones. Along $\vec{b}^*$, the fifth, ninth, and tenth reflections, indicated by arrows, are more intense, they would correspond to the basic reflections of the subsystems, 0200−0002 and 0400, respectively. This theoretical pattern differs from the experimental ones by the r value which is exactly ${}^9/_5$. It implies that the satellites resulting from the interaction of the two subsystem are perfectly superimposed. As an example the $0\bar{6}04$ and $030\bar{1}$ reflections give rise to a single reflection which would be indexed 060 in the approximated commensurate supercell. In the experi-

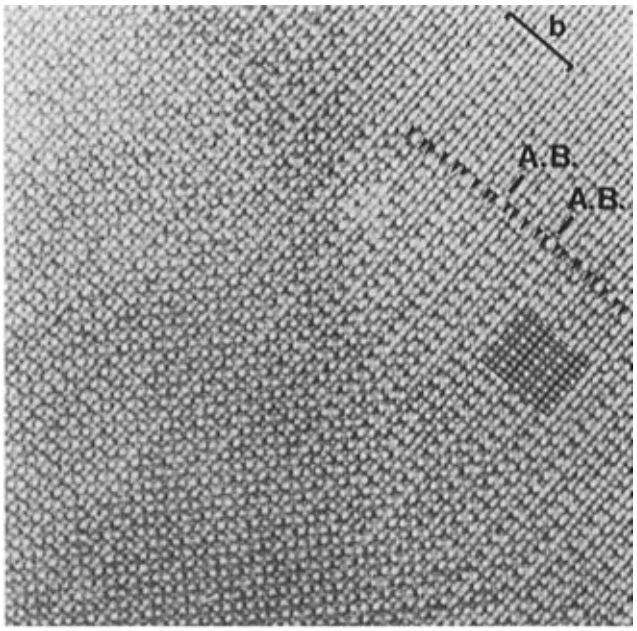

Figure 8. Typical (001) HREM image: the contrast is characterized by the existence of alternated rows of bright and gray dots. The theoretical image calculated for a focus value close to −110 nm and a crystal thickness of 4.7 nm is superimposed. The three rows of smaller dots, indicated by arrow, are correlated to the thallium rows running along $\vec{a}$. Antiphase boundaries are common features.

mental patterns, depending on *r*, such reflections are more or less split (Figure 3).

As could be expected from the lamellar character of this compound, the [001] orientation is by far the most common orientation of the crystallites. Unfortunately, this projection direction provides almost no information on the way the slabs are stacked along *c*. Nevertheless, the image calculations based on our hypothetical model are a helpful guide for interpreting the experimental images. The theoretical images were calculated for the atomic parameters displayed in Table 2, varying the focus values and crystal thicknesses. To understand the contrast in correlation with the different layers (strontium-based rock-salt layer, hexagonal cobalt layers, and the intercalated thallium layers), the calculations were carried out for two extreme models and a third one corresponding to the actual composition. The first limit model corresponds to $Tl_{0.66}[SrO]_{1.12}CoO_2$ where all the possible thallium sites are fully occupied and the second one to the hypothetical thallium-free compound $[SrO]_{1.12}[CoO_2]$. The third model corresponds to a partial occupancy of thallium and strontium sites, according to the formula $Tl_{0.41}[(Sr_{0.9}\square_{0.1})O]_{1.12}CoO_2$. In that case, the corresponding calculated images are very similar to those obtained in the limit model $Tl_{0.66}[SrO]_{1.12}CoO_2$.

The two through-focus series of $[SrO]_{1.12}[CoO_2]$ and $Tl_{0.41}[(Sr_{0.9}\square_{0.1})O]_{1.12}CoO_2$ are compared in Figure 7a,c, respectively, for a crystal thickness of 4.7 nm.

The images calculated for the thallium free model $[SrO]_{1.12}[CoO_2]$ (Figure 7a) are characterized by a modulated variation of the contrast along $\vec{b}$. For focus values where the high electron density zones are highlighted (for example, for focus values close to −50 and −110 nm), the contrast can be described in terms of rows, parallel to $\vec{b}$ where three adjacent very bright large dots are surrounded by two medium bright dots and followed by five small gray dots. This contrast is

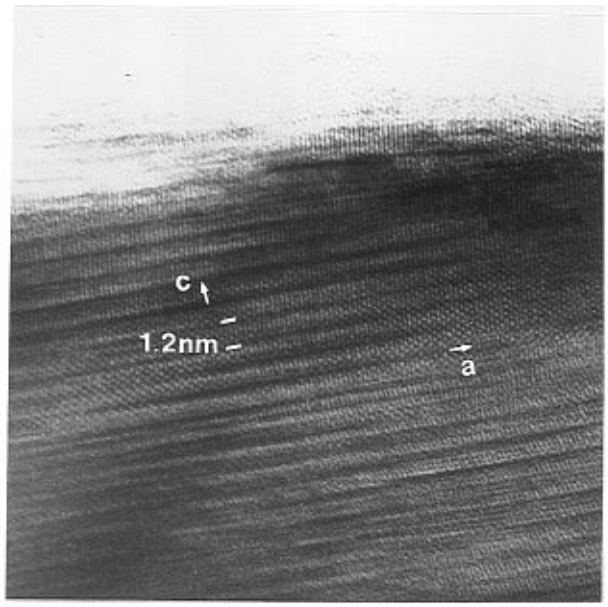

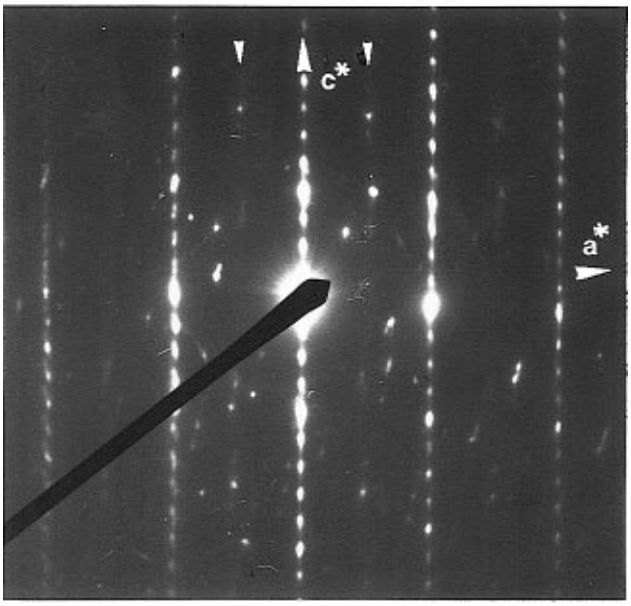

Figure 9. (010) HREM image of $Tl_{0.41}[(Sr_{0.9}\square_{0.1})O]_{1.12}CoO_2$ and corresponding ED pattern.

shifted by $(a + b)/2$ leading to a centered image in agreement with the C-type lattice. In terms of projected potential, these groups of three dots are correlated to the three positions where Sr, Co, and O positions are exactly projected over the same point (Figure 7b).

The theoretical images calculated for the thallium compound $Tl_{0.41}[SrO]_{1.12}CoO_2$ (Figure 7c) show that, for several focus values, the contrast is significantly modified by the intercalation of thallium. It mainly consists in the loss of the modulated brightness of the dots along $\vec{b}$. The most striking effect is the disappearance of the three adjacent bright dots, whatever the focus value is; in that way, the three dots do not exhibit anymore a similar brightness but the medium one is highlighted or darkened with regard to the two others. Such an effect results from the superposition of one Tl over the medium position (single arrow in Figure 7c,d, respectively). As an example for a focus value of −110 nm, these atomic columns appear as a single row of gray dots surrounded by two rows of very bright dots with

regard to the other ones. In the same way, a double row of staggered bright dots of equal brightness is now clearly visible in the images, corresponding to the second group of thallium (double arrow in Figure 7c,d, respectively). Though these calculations cannot be considered as an absolute proof of the rightness of our model, they can be used for interpreting the images and the nature of the atomic columns, except the stacking principle.

An example of experimental images where the focus is evaluated close to −110 nm is given in Figure 8, which show that the observed contrast fits well with the theoretical one calculated for our model proposed for $Tl_{0.41}[SrO]_{1.12}CoO_2$. One clearly observes the existence of a single row of small dots (single arrow), between two rows of bright dots and the existence of two adjacent rows of equal brightness (two adjacent arrows). The sequence, along $\vec{b}$, of the rows parallel to $\vec{a}$ is then bright−gray−bright−two gray, in agreement with the simulated images. The three rows of gray dots (indicated by arrow) are correlated to thallium rows.

In fact, the images show that such a perfect periodic contrast is not observed within the whole matrix but that the very regular arrangement of dots only arises at short distances. It is locally broken by the existence of "antiphase" boundaries correlated to the sequences of the thallium rows along $\vec{b}$; the sequence double−single−double−single rows is locally defective with the existence of two adjacent double rows of staggered thallium. Such a feature involves concomitantly a local variation of the periodicity along $\vec{b}$. These phenomena are shown in Figure 8.

As mentioned above, [010] orientations were rarely observed; moreover, when this occurs, the contrast is hardly interpretable because the thin lamellae are often distorted. A [010] ED pattern is shown in Figure 9, with the corresponding image. From such images, it appears that few defects are observed and that the stacking along $\vec{c}$ is rather regular. However, it can be observed that the layers are rather distorted, probably due to an irregular intercalation of the thallium atoms. This distortion originates the weak diffuse streaks, parallel to $\vec{b}^*$, which show that the C-type lattice is in fact violated in a rather random way.

Concluding Remarks

A misfit layer oxide $Tl_{0.41}[(Sr_{0.9}\square_{0.1})O]_{1.12}CoO_2$ has been synthesized for the first time, showing the great analogy of this system with the sulfides $[MS]_{1+x}[TS_2]$.

This behavior of the system Tl−Sr−Co−O, very different from those observed for the Tl−Sr−Cu−O system opens the route to the exploration of new bidimensional oxides that will be studied for their magnetic properties.

The investigation of the existence range of this new phase is in progress. It shows that the nonstoichiometry phenomena in these oxides are so far not understood, as well for the thallium sites as for the strontium sites whose occupancy may be correlated, suggesting the possible existence of various members with the generic formula $Tl_y(Sr_{1-\delta}O)_{1+x}CoO_2$. The substitution of calcium for strontium is also studied to modify the parameters of these phases and especially to change the "1 + x" term.

Further experiments, dealing with crystal growth, but also with powder X-ray synchrotron diffraction are in progress to precisely determine the structures of these compounds.

Acknowledgment. The authors wish to thank Prof. H. Leligny for valuable discussions during the present work.

CM9601446